X-ray diffuse scattering from icosahedral Al-Pd-Mn quasicrystals

M. J. Capitan
ESRF, Avenue des Martyrs, Boîte Postale 220, 38043 Grenoble, France

Y. Calvayrac and A. Quivy
CECM-CNRS, 15 rue Georges Urbain, 94407 Vitry, France

J. L. Joulaud
ESRF, Avenue des Martyrs, Boîte Postale 220, 38043 Grenoble, France

S. Lefebvre
LURE, Bâtiment 209, Boîte Postale 34, 91898 Orsay, France

D. Gratias
LEM-CNRS/ONERA, Boîte Postale 72, 92322 Châtillon, France
(Received 28 December 1998; revised manuscript received 16 March 1999)

The diffuse scattering of the thermodynamically stable icosahedral phase *i*-AlPdMn has been studied by means of x-ray-diffraction technique. The overall diffuse intensity shows two main characteristics: (1) the global diffuse scattering intensity map is well taken into account by a Huang effect in the formalism developed by Jarić and Nelson [Phys. Rev. B **37**, 4458 (1988)] for icosahedral symmetry which reproduces at once both the ''background'' diffuse intensity and the profile shape around the Bragg peaks; (2) the intensity level of the diffuse scattering is crucially dependent on the chemical composition of the sample; it varies drastically from almost free diffuse scattering samples close to an ''ideal'' composition, up to an overall increase by a factor of 20 of the diffuse scattering for samples with an off-stoichiometry less than 0.5% in manganese and palladium content. The relative shapes of the diffuse scattering contours around the Bragg peaks are qualitatively fairly well reproduced using the sole phason-phason term of hydrodynamical modes in the formalism of Jarić and Nelson [Phys. Rev. B **37**, 4458 (1988)], suggesting that phasons in these *F*-type icosahedral quasicrystals induce minor relaxations in the atomic positions surrounding the flip locations. [S0163-1829(99)06729-6]

I. INTRODUCTION

After the discovery of quasicrystals[1] a large number of studies have been performed with the aim of determining the atomic structure of these intriguing materials. Stable icosahedral phases like *i*-AlPdMn and *i*-AlCuFe have shown to be of exceptional high structural quality — the average peak widths measured on single grain samples are roughly only twice larger than those observed in the best silicon crystals — as compared to usual intermetallic structures. However, a close examination of the diffraction peaks by high-resolution diffraction show typical peak shapes related to a Huang scattering effect that has been theoretically discussed short after the discovery of quasicrystal by Bak[2] and Jarić and Nelson.[3] Over the last years, an intensive theoretical research has developed in the field of diffuse scattering in icosahedral quasicrystalline phases in an increasing number of studies.[4–10]

In contrast with this substantial amount of theoretical works, the number of experimental studies has remained relatively low[11–16] because of the high level of measurement accuracy it requires for being soundly extracted from the many possible experimental artifacts that can hide the phenomenon. Presently available results shows some discrepancies in both the results and interpretations obtained by the various authors according to which technique and which samples they used. On one hand, the diffuse intensity in the vicinity of the Bragg peaks has been studied[11–13] on large Al-Pd-Mn single crystals. They showed the presence of strong diffuse scattering intensity with specific shapes that could be well reproduced in the formalism of Jarić and Nelson.[3] Other studies have even evidenced a weakly modulated diffuse background signal that has been attributed to an apparently significant chemical and geometrical partial disorder.[16] Both features have been considered as intrinsic of icosahedral structures. On the other hand, high-resolution x-ray-diffraction studies[14,15] do not show evidence of diffuse intensity. However, they show numerous well-resolved low intensity Bragg peaks—whose number increases with the resolution since the Fourier transform of a quasiperiodic object is a dense set of peaks—are present in the same area of the reciprocal space, and that could be the origin of the diffuse signal of the neutron studies. The existence at room temperature of an icosahedral phase free of defects should indicate an extremely high structural stability. This point justify the importance of the diffuse scattering studies.

The present paper reports a set of experiments performed at the European Synchrotron Radiation Facility (ESRF-Grenoble, France) motivated by our concern of clarifying this apparent contradiction between neutrons and x-ray-diffraction studies in performing a data collection through a

high-resolution scan including at once both the shapes of the Bragg peaks and the overall diffuse scattering in an unique intensity map for two different samples of close chemical composition. Using the ESRF allowed us to take advantage of the possibility of combining a high-resolution configuration with a brilliance that is still comfortable for recording diffuse scattering maps of a very fine mesh within quite an extended part of a plane in reciprocal space.

II. EXPERIMENTAL DETAILS

Two single grains of the icosahedral phase of the ternary Al-Pd-Mn alloy with tiny differences in their composition, were grown from the melt by the Czochralski method using a fivefold axis seed quasicrystal. The final samples were 4 mm thick disks with a diameter close to 1 cm. They were cut perpendicularly to the growth direction from the mother single grain that had been previously annealed at 1073 K. The disks were mechanically polished and subsequently annealed at 873 K in high vacuum in order to relax the internal stresses produced during the polishing. The samples were rapidly cooled down in order to avoid the formation of secondary phases. The final compositions of the two samples as obtained by inductively coupled plasma (ICP) emission spectrometry are $Al_{70.7}Pd_{21.4}Mn_{8.2}$ (sample 1) and $Al_{70}Pd_{21}Mn_8$ (sample 2), respectively, (compositions are given in at. %).

Careful preliminary synchrotron x-ray experiments were made in order to scan for possible residual phases leading us to the conclusion that both disks were single phased. A close examination of the linewidths of 18 peaks that are characteristic of the icosahedral phase revealed that the quasicrystalline quality of the samples was excellent.

In order to record the x-ray diffuse scattering in a high-resolution configuration and with a large dynamical detection range, we took advantage of the high brilliance offered by the ID01 beamline of the ESRF. The anomalous scattering beam line ID01,[17] is equipped with a six-circle goniometer setup, which has been used in our experiments. The beam line optics use a double-crystal monochromator [Si(311)] with fixed exit. The first crystal is nitrogen cooled. The detection was done by means of a NaI scintillator detector combined with a Si(111) crystal analyzer. The use of this analyzer crystal increases the angular resolution and the signal-to-background ratio by suppressing fluorescence. The instabilities of the incident beam are automatically corrected for by a monitor detector which records diffuse scattering from a Kapton foil. The data are recorded as angular scans in a vertical scattering plane.

The incident energy was adjusted to 6.450 keV on the basis of extended x-ray absorption fine structure (EXAFS) reference spectra from a Mn foil. The accuracy of the energy determination is 1 eV and the wavelength resolution $\triangle\lambda/\lambda$ of the triple-axis configuration used is 0.9×10^{-3}. In order to tune to this energy we operated the beam within the third harmonic of a wiggler with a gap of 36 mm (undulator regime). The beam size used at the sample position was 0.2 mm (vertical)$\times$3 mm (horizontal).

From the crystallographic point of view, icosahedral quasicrystalline structures are best described as irrationally oriented three-dimensional (3D) cuts of 6D periodic objects. The 3D cut space represents the actual physical space being usually called the parallel space; the perpendicular 3D space, complement in 6D of the physical space is called the perpendicular space. Thus the quasicrystal lattice vectors V are 6D vectors that decompose into two 3D components $V=(V_\parallel,V_\perp)$, where $V_\parallel$ is a vector of the physical space, and $V_\perp$ its image in the perpendicular space. In the notations of Cahn *et al.*[18], the 6D lattice vectors are defined by six integers $V=(h/h',k/k',l/l')$ such that, irrespective of a global scale factor, $V_\parallel=(h+h'\tau,k+k'\tau,l+l'\tau)$ and $V_\perp=(h'-h\tau,k'-k\tau,l'-l\tau)$, where $\tau=(1+\sqrt{5})/2$ is the golden mean. The icosahedral reflections can be classified into families of equal length wave vectors, noted (N,M), where the two integers N and M, given by $N=h^2+k^2+l^2+h'^2+k'^2+l'^2$ and $M=h'^2+k'^2+l'^2+2(hh'+kk'+ll')$ are such that $q_\parallel^2=N+M\tau$ and $q_\perp^2=N\tau-M$.

We chose the convention of indexing the (18,29) Bragg peak along the fivefold axis perpendicular to the surface as (1/2,2/3,0/0). The part of the reciprocal space measured belongs to the [0/0, 0/0, 0/2] zone axis. The window selected for the scans is shadowed in Fig. 1 and it corresponds to a part of reciprocal space around the (8,12) Bragg peak (0/0, 2/2, 0/0). The scan step used ($\Delta q=5\times10^{-3}$ Å^{-1}) was chosen as two times the full width at half maximum (FWHM) of the experimental resolution function in order to recover complete information on the selected part of reciprocal space with a minimum of overlap. Because we are interested here in low intensity signals, the experimental data (see, for instance, Fig. 2) are presented in this paper on a logarithmic scale.

III. EXPERIMENTAL RESULTS

The experimental intensity map recorded with sample 1 is shown in the left part of Fig. 2. The frame of the map contains the three peaks noted (8,12) (noted *A* in the lower left hand corner), (11,16) (noted *B* at intermediate heights at the right-hand edge of the map), and (14,21) (noted *C*, higher up and towards the center of the map). These three peaks are used as spatial reference poles. Other additional low-intensity peaks (not explicitly indexed on the figure for not overloading the drawing) can also be observed which all correspond to well-defined icosahedral peaks. Two important features can be noticed:

(1) There are zones in reciprocal space, between Bragg peaks, where the diffuse background intensity is extremely low, down to the standard background noise.

(2) The Bragg peaks exhibit specific line shapes which differ from one peak to another.

To appreciate the experimental pertinence of these features, the same portion of the reciprocal space region for a perfect silicon single crystal has been recorded.[19] It was observed that the lowest background signals obtained on the silicon sample fits those recorded for the quasicrystal: for example, at a distance of 0.25 Å^{-1} from the Bragg peak (8,12) in the quasicrystal the intensity drops down the detection limit (6 count/s) as it does in the silicon sample. The only difference between the two maps is a higher density of Bragg peaks in the icosahedral case which shrinks the regions free of diffuse scattering.

The peak shapes of silicon are different from those of the quasicrystal: in the former case, the Bragg peak intensity is

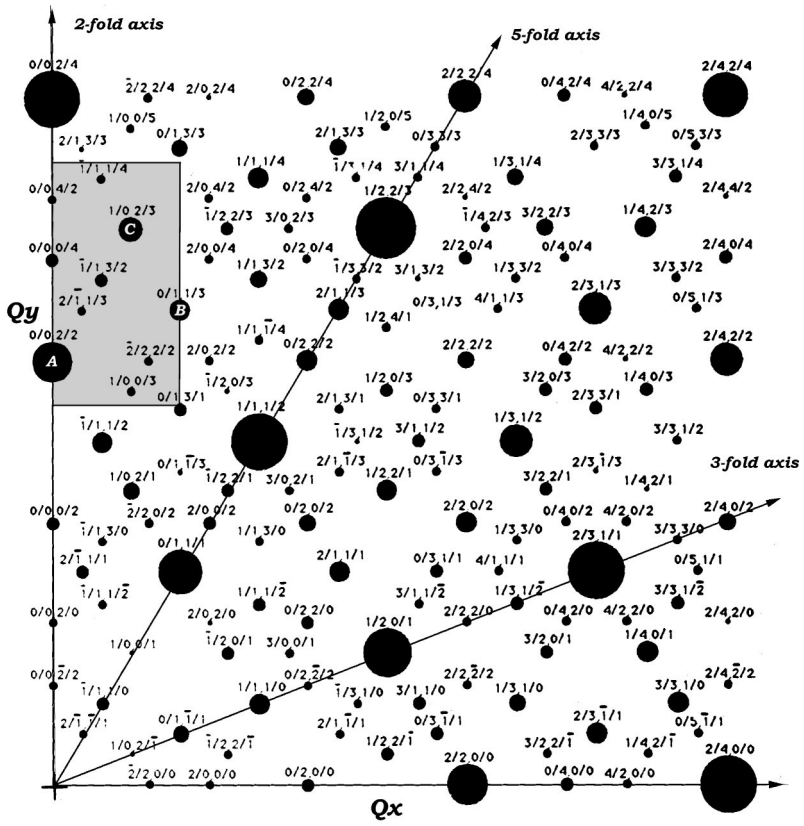

FIG. 1. Diffraction map in a mirror plane [unit vectors $u_x=(1/0,0/0,0/0)$ and $u_y=(0/0,1/0,0/0)$] of an icosahedral *F*-type quasicrystal. The region of the reciprocal space investigated in this study is delimited by the dashed box. The (8,12), (11,16), and (14,21) poles used as reference in the article are noted, respectively, *A*, *B*, and *C*. The reflections in this plane are characterized there by *x* and *y* components and have a zero *z* component.

spread out along the ω direction (because of mosaicity) whereas, in the *i*-AlPdMn quasicrystal, it extends mainly along the threefold directions. In order to determine the 3D extension of this diffuse region, additional scans around the (0/0, 2/2, 0/0) Bragg peak have been performed. The polar cross section along directions parallel to the high symmetry axes, and away from the Bragg peaks are shown in Fig. 3. The open circles in Fig. 3 correspond to the diffuse intensity of sample 1 and the full circles to the one of sample 2. In both cases, maxima of intensity are observed as elongated diffuse intensity tails issued from the nearby Bragg reflections along a threefold direction. The overall shape in reciprocal space of this diffuse intensity region was determined by means of additional scans in a mirror plane perpendicular to the one under study. Observing the same FWHM (full width a half maximum) for the diffuse scattering signal in two transverse directions, we conclude that the diffuse intensity is elongated along threefold directions.

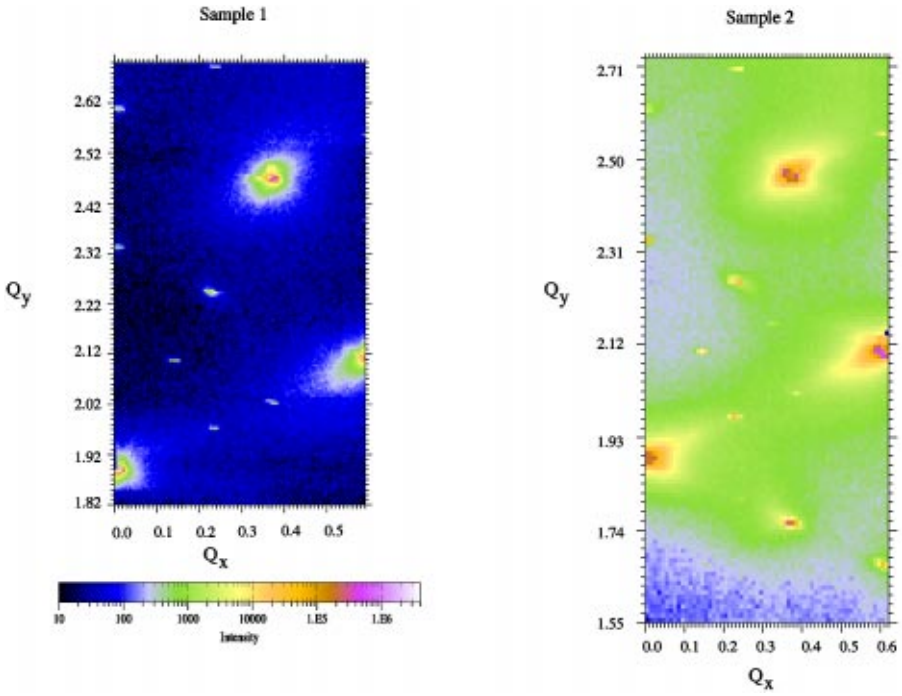

FIG. 2. (Color) Measured intensity map for sample 1 (on the left) and sample 2 (on the right) of both *i*-AlPdMn single grains. The intensity scale used is the same for both samples and is presented on a logarithmic scale for better showing the peak shapes in the low diffuse intensity regions. Reciprocal length scales along *x* and *y* are given in Å^{-1}.

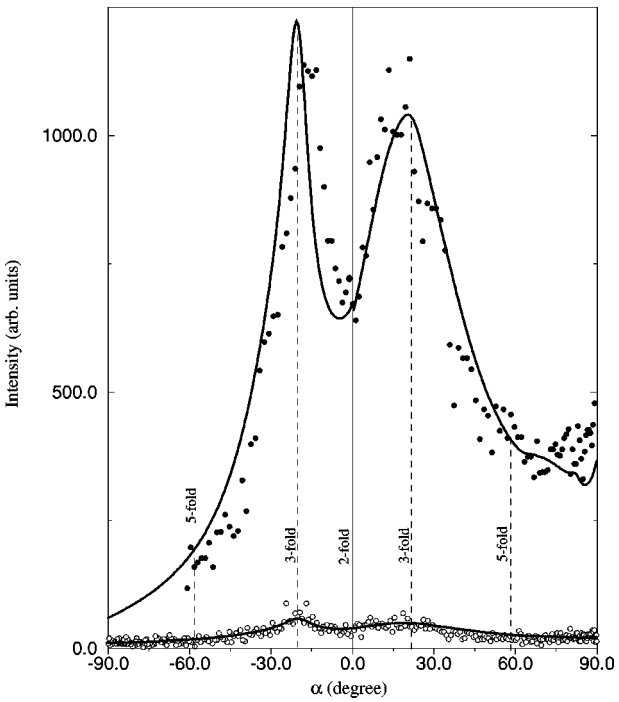

FIG. 3. Cross section in the x,y plane of the diffuse scattering intensity as a function of the polar angle on a ring away from the Bragg peaks around the (8,12) reflection. Open circles correspond to sample 1 and full circles to sample 2. The full lines correspond to the numerical fits as explained in the discussion section.

Sample 2 differs from sample 1 by less than 0.5% in Mn and Pd content. It has been prepared and studied in the very same way with the unique difference in the experimental setup that the step size of the mesh scan has been doubled in order to reduce the measuring time and to scan a slightly larger portion of reciprocal space in the Q_y direction. To preserve the same ratio between the step and the resolution, the incident energy was adjusted to 11.0 keV by reference to the EXAFS spectrum of the Mn foil. The resolution in this setup with a InSb(1,1,1) analyzer crystal is 2.8×10^{-3} Å^{-1}. The data obtained in the two different configurations could be put on a common basis of normalization by using the integrated intensities from a silicon single crystal. The resulting corrected diagram is presented on the right-hand side of Fig. 2. Although the Bragg peak intensities[20] are the same for both samples, the overall level of diffuse scattering in sample 2 is considerably higher, by an overall factor of 20, in sample 2 than in sample 1. Nevertheless, the anisotropic shapes of the Bragg peaks are qualitatively the same. In particular, the ''streaks'' along the threefold direction are even more clearly visible in sample 2.

IV. DISCUSSION

Our experiments show that the diffuse intensity depends crucially on composition. This can be attributed to off-stoichiometry defects introduced in the sample 2. In that scheme, sample 1 would be closest to an ''ideal'' well-defined composition for which the diffuse intensity drops in some regions of the reciprocal space to the level of the experimental background noise. To that aspect, the quasicrystal behaves as a remarkably well-ordered structure as compared to usual ordered fcc-based metallic alloys. Both the very sharp stoichiometry domain and the absence of Laue diffuse scattering are consistent with quasicrystals being typical examples of complex intermetallic definite compounds.

The peak shapes appear to be robust features with respect to compositional fluctuations. This raises the question of the structural origin of these shapes as atomic displacements rather than chemical substitution. As will be shown below, they can all be fairly reproduced within the theoretical framework in 6D space proposed by Jarić *et al.*[3,4,6] using the Huang effect in icosahedral structures. Assuming ''elastic''-type basic interactions, they were able to calculate the diffuse scattering intensity that would result from a statistical distribution of interacting phonons and phasons in a perfect icosahedral phase at thermal equilibrium. For the icosahedral symmetry, the 6×6 hydrodynamical matrix $\hat{C}$ decomposes into 3D submatrices depending on five independent elastic moduli. The diffuse scattering amplitude $I(\vec{Q}_\parallel+\vec{q}_\parallel)$, at offset $\vec{q}_\parallel$ from a 6D Bragg peak $\vec{Q}=(\vec{Q}_\parallel,\vec{Q}_\perp)$, is given by

$$I(\vec{Q}_\parallel+\vec{q}_\parallel)=({}^t\vec{Q}_\parallel,{}^t\vec{Q}_\perp)\hat{\mathbf{C}}^{-1}(\vec{q}_\parallel)\begin{pmatrix}\vec{Q}_\parallel\\ \vec{Q}_\perp\end{pmatrix}. \tag{1}$$

The hydrodynamical matrix $\hat{C}(\vec{q}_\parallel)$ is written as

$$\hat{\mathbf{C}}(\vec{q}_\parallel)=\begin{pmatrix}\hat{\mathbf{C}}_{\parallel,\parallel} & \hat{\mathbf{C}}_{\parallel,\perp}\\ \hat{\mathbf{C}}_{\perp,\parallel} & \hat{\mathbf{C}}_{\perp,\perp}\end{pmatrix}, \tag{2}$$

where $\hat{\mathbf{C}},_{\parallel,\parallel}$, $\hat{\mathbf{C}}_{\parallel,\perp}$ and $\hat{\mathbf{C}}_{\perp,\perp}$ are the 3×3 matrices containing the phonon-phonon, phonon-phason, and phason-phason interactions, respectively, as explicitly given in the Appendix.

The phonon-phonon hydrodynamical matrix depends on the elastic constants μ and λ. The phonon-phason matrix depends on the coupling constant K_3 and the phason-phason matrix on the parameters K_1 and K_2 similar to elastic constants in perpendicular space. Widom[5] has made a very interesting and exhaustive study of the above hydrodynamic matrix by calculating its eigenvalues and eigenvectors: regions can be defined in the (K_1,K_2,K_3) space that would eventually lead to specific instabilities along fivefold (so-called vertex instability), threefold (face instability), and twofold (edge instability) directions. The calculated diffuse scattering maps in reciprocal space typical of these three cases for typical values of the coupling constants is presented in Fig. 4. For the vertex instability, the diffuse scattering around the Bragg peaks is elongated along the fivefold direction, along the twofold directions for the edge instability and along the threefold directions for the case of the face instability. Instead of confining the calculation of the diffuse scattering given by Eq. (1) around each reflection independently, we summed up, at each point of the reciprocal space, the contribution issued for all reflections of the plane. A comparison of this calculation with our experimental results (see Fig. 2 and the cross section shown in Fig. 3) shows that the diffuse scattering observed in our samples corresponds best to coupling constants belonging to the threefold (face) instability region.

To evaluate the relative contribution of the three types of modes (phonon-phonon, phason-phonon, and phason-phason

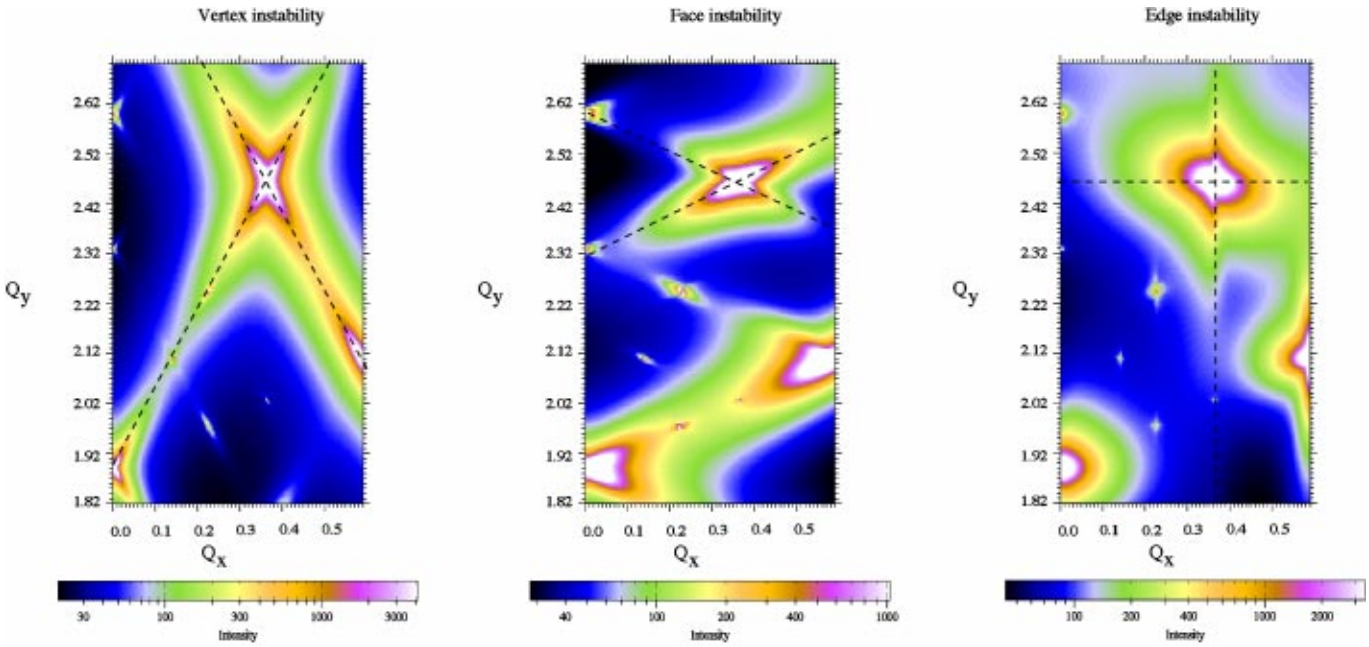

FIG. 4. (Color) Calculated diffuse scattering intensity (logarithmic scale) for the three kinds of instabilities described by Widom (Ref. 5), vertex ($K_1=1$, $K_2=0.7$), face ($K_1=1$, $K_2=-0.7$), and edge ($K_1=1$, $K_2=0$, $K_3\neq 0$) in the reciprocal region corresponding to the experimental scans.

couplings) the intensity for two normalized (20,32) and (40,60) Bragg peaks with significantly different $Q_\perp$ values has been compared in sample 2 where the diffuse intensity is more pronounced. As shown in Fig. 5, the relative intensity at the feet of the Bragg peaks increases with the $Q_\perp$ length whereas the dependence on the $Q_\parallel$ parameter is much weaker. Hence, the observed diffuse scattering in sample 2 is mainly dominated by the phason-phason mode: most of the disorder revealed by diffuse scattering in this sample can be attributed to phason defects. In a good approximation, the diffuse scattering intensity in the vicinity $\vec{q}_\parallel$ of the Bragg peak $(\vec{Q}_\parallel,\vec{Q}_\perp)$ is well reproduced by

$$I(\vec{q}_\parallel)\approx {}^t\vec{Q}_\perp \hat{\mathbf{C}}^{-1}_{\perp,\perp}(\vec{q}_\parallel)\vec{Q}_\perp . \tag{3}$$

A least-squares fit of the experimental data has been performed for both samples using Eq. (3) to obtain the simulated diffuse intensity map shown in Fig. 6. Because of the large dynamical range of the signal (the ratio of the peak intensity to the background noise is approximately 10^8), we used a logarithmic[21] merit function χ^2:

$$\chi^2=\frac{1}{N_{\rm pts}-N_{\rm par}}\sum_{i=1}^{N_{\rm pts}}\{\log_{10}[I_c(i)]-\log_{10}[I_m(i)]\}^2,$$

where I_m and I_c are, respectively, the measured and calculated intensities at the ith of the $N_{\rm pts}$ scan points and $N_{\rm par}$ is the number of fitting parameters. The peak contributions are considered to be proportional to the maximum peak intensities of each peak. The free parameters in the pure phason mode are a global scale parameter and the ratio K_2/K_1. The accuracy of the parameters have been estimated in changing one parameter with the other parameters relaxed until χ^2 has increased by $1/(N_{\rm pts}-N_{\rm par})$ from its minimum value.[22]

The fitted K_2/K_1 ratio has been found to be $K_2/K_1=-0.50\pm0.02$ for sample 1 with $\chi^2=0.19$ and $K_2/K_1=-0.60\pm0.02$ for sample 2 with $\chi^2=0.09$. These values are consistent with those reported by Boudard *et al.*[11] who

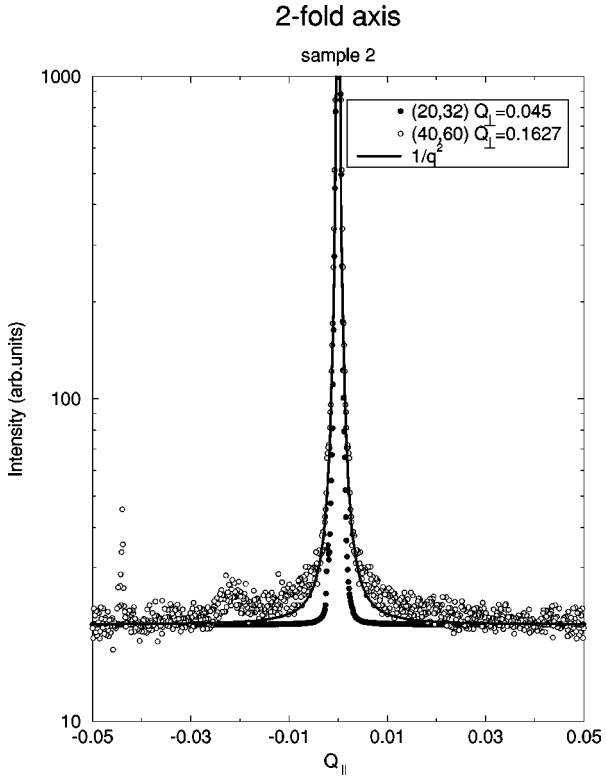

FIG. 5. Decay of the diffuse scattering intensity along the twofold direction around the Bragg peaks (20,32) (full circles) and (40,60) (open circles) with significantly different $Q_\perp$ values in sample 2. The maximum of intensity, out of range in the figure, has been arbitrarily normalized to 35 000 counts. The full line curve corresponds to a standard $1/q^2$ decay.

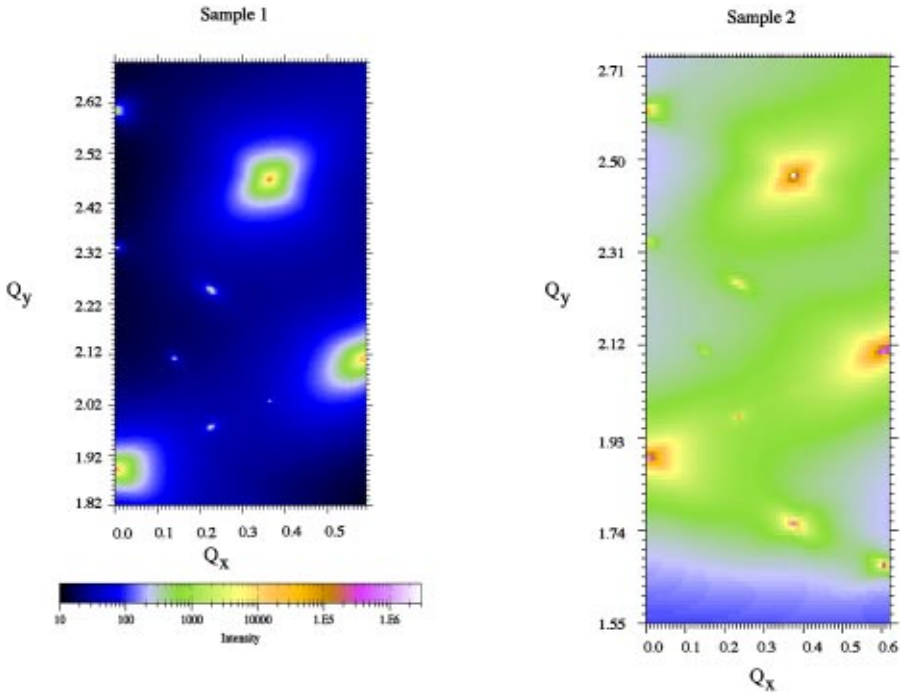

FIG. 6. (Color) Diffuse scattering intensity resulting from the fit of the measured data. The fit parameters and the conditions are described in the text. The intensity scale is the same for both experimental (Fig. 2 and cross section in Fig. 3) and calculated data.

found $K_2/K_1=-0.52$ in single peak analyses for a sample with a slightly different composition. This suggests the threefold (face) phason mode to be a common feature between all these samples, which is robust with respect to composition fluctuations.

On the contrary, the scaling factor varies drastically from sample 1 to sample 2 by a factor of 20. Such a huge variation cannot be due to differences in the annealing temperatures between the two samples which were heat-treated in the same way. It was observed that the overall fit is better[23] for sample 2 than for sample 1. Indeed, even with a logarithmic merit function, the least-squares fit technique is still mostly driven by the large signals, i.e., close to Bragg peaks, at the expense of the small signals of the diffuse wings. As the Bragg peak intensities are identical for both samples, this tendency to bias the fit values must be stronger in sample 1 than in sample 2. A small improvement of the fit, decreasing χ^2 to 0.17—which is still way above the value of 0.09 obtained for sample 2—is obtained by introducing the remaining instability parameters in the minimization.

In fact, sample 1, being closer to the ''ideal'' composition (as revealed by its very low background diffuse intensity), may contain fewer phasons defects than sample 2. Therefore, phonon-phonon and phason-phonon coupling effects—that could have been hidden in the case of sample 2 that is off-stoichiometry—could become detectable in sample 1. The fitted values for the elastic moduli are then $K_1=0.97\pm0.02$, $K_2=-0.52\pm0.01$, and $K_3=-3.62\pm0.04$. The μ and λ values have a large inaccuracy because they are dependent on the inverse of an ill-conditioned or nearby singular matrix (see, for instance, Ref. 9). The following fitted values are simply orders of magnitude: $\mu\approx30\pm10$ GPa and $\lambda\approx-50\pm20$ GPa. The negative value of λ indicates that, despite the poor accuracy of the present calculation, the Poisson coefficient $\nu=\lambda/2(\lambda+\mu)$ is expected to be larger in these materials than in the usual periodic metallic alloys. Although it is not possible to draw any sound conclusions because of the inaccuracy of these values, the opposite signs obtained for the elastic constants can be taken as an indication of a large Poisson coefficient in these materials.

V. CONCLUSIONS

We have shown that diffuse scattering intensity in *i*-AlPdMn quasicrystals is well reproduced in all its parts as an ''icosahedral'' Huang effect, which is described in Ref. 3 in the framework of a Landau-Ginsburg approach. A composition exists where the Laue-type diffuse intensity reduces to the natural background noise, hence confirming the idea that quasicrystals have a narrow, well-defined composition range where they exhibit an exceptionally high degree of chemical order. These experiments have shown, however, that the diffuse intensity is strongly dependent on the composition: it increases by a factor of 20 when the sample composition is slightly modified with respect to the ''ideal'' icosahedral composition by less than 0.5% change in Mn and Pd content. This high sensitivity to composition fluctuation could explain the discrepancies found in the literature between the various groups who use different techniques on different samples. In particular, it might be plausible that the large samples needed for neutron diffraction present small composition gradients around the ideal composition that would be responsible—together with the inherent low-resolution of the apparatus—for the diffuse signal reported by Caudron *et al.*[16]

Apart from this overall scaling factor, the anisotropic peak shapes do not change significantly with composition: they have well-defined characteristics depending on the peaks themselves. They are well reproduced as a Huang effect adapted for the icosahedral case long ago by Jarić and Nelson.[3] Our results follow from the icosahedral symmetry and do not suggest the necessity of the proximity of a phase transformation. In particular, the intriguing diffuse scattering described as ''streaks'' along the threefold directions are properly reproduced by the above calculations and are there-

fore essentially built-in features of the icosahedral symmetry. They are, to some extent, the signature of the true icosahedral nature of these solids.

ACKNOWLEDGMENTS

The authors wish to thank M. Bessière, J. Alvarez, and M. Quiquandon for their constant and inestimable help in the development of this work. M.C. would like to thank G. Coddens for a very accurate reading of the manuscript and for useful discussions. We thank the ESRF for facilitating for us the use of its installations for the realization of this work.

APPENDIX

The elastic constants used here can be related with the m_i constants introduced by Jarić *et al.*[3] by the relationships: $K_1=m_3/3$, $K_2=m_4/2\sqrt{5}$, $K_3=m_5/2\sqrt{15}$, $\lambda=\sqrt{2}m_2/\sqrt{15}$ and $\lambda=(\sqrt{5}m_1-m_2)/2\sqrt{30}$.[3,5] Let $\vec{q}_\parallel=(q_1,q_2,q_3)$ be the running offset vector from a Bragg reflection in reciprocal space. The hydrodynamical 3×3 matrices are defined by

$$\hat{\mathbf{C}}_{\parallel,\parallel}(\vec{q}_\parallel)=\frac{1}{k_BT}\begin{pmatrix}\delta_1 & (\mu+\lambda)q_1q_2 & (\mu+\lambda)q_1q_3\\ (\mu+\lambda)q_2q_1 & \delta_2 & (\mu+\lambda)q_3q_2\\ (\mu+\lambda)q_3q_1 & (\mu+\lambda)q_3q_2 & \delta_3\end{pmatrix}, \tag{A1}$$

with $\delta_i=\mu|q|^2+(\mu+\lambda)q_i^2$,

$$\hat{\mathbf{C}}_{\parallel,\perp}(\vec{q}_\parallel)=\frac{K_3}{k_BT}\begin{pmatrix}\gamma_1 & 2\tau^{-1}q_1q_2 & -2\tau q_1q_3\\ -2\tau q_1q_2 & \gamma_2 & 2\tau^{-1}q_3q_2\\ 2\tau^{-1}q_3q_1 & -2\tau q_3q_2 & \gamma_3\end{pmatrix}, \tag{A2}$$

with $\gamma_i=q_i^2-\tau q_{i+1}^2+\tau^{-1}q_{i+2}^2$,

$$\hat{\mathbf{C}}_{\perp,\perp}(\vec{q}_\parallel)=\frac{K_2}{k_BT}\begin{pmatrix}\phi_1 & 2q_1q_2 & 2q_1q_3\\ 2q_2q_1 & \phi_2 & 2q_2q_3\\ 2q_3q_1 & 2q_3q_2 & \phi_3\end{pmatrix}, \tag{A3}$$

with $\phi_i=(K_1/K_2)|q|^2-|q|^2/3+\tau^{-1}q_{i+1}^2-\tau q_{i+2}^2$.

[1] D. Shechtman, I. Blech, D. Gratias, and J. W. Cahn, Phys. Rev. Lett. **53**, 1951 (1984).
[2] P. Bak, Phys. Rev. B **32**, 5764 (1985).
[3] M. V. Jarić and D. R. Nelson, Phys. Rev. B **37**, 4458 (1988).
[4] M. V. Jarić and U. Mohanty, Phys. Rev. B **37**, 4441 (1988).
[5] M. Widom, Philos. Mag. Lett. **64**, 297 (1991).
[6] M. V. Jarić and U. Mohanty, Phys. Rev. Lett. **58**, 230 (1987).
[7] Y. Ishii, Phys. Rev. B **45**, 5228 (1992).
[8] Y. Ishii, Phys. Rev. B **39**, 11 862 (1989).
[9] T. C. Lubensky, S. Ramaswamy, and J. Toner, Phys. Rev. B **32**, 7444 (1985).
[10] P. A. Kalugin, A. Y. Kitayev, and L. S. Levitov, J. Phys. (France) Lett. **46**, L601 (1985).
[11] M. Boudard, M. de Boissieu, M. Audier, S. Kycia, A.I. Goldman, H. Hennion, R. Bellissent, and M. Quilichini (unpublished).
[12] M. de Boissieu, M. Boudard, R. Bellissent, S. Kycia, A. I. Goldman, C. Janot, and M. Audier, Phys. Rev. Lett. **75**, 89 (1995).
[13] M. Boudard, M. de Boissieu, A. Letoublon, H. Hennion, R. Bellissent, and C. Janot, Europhys. Lett. **33**, 199 (1996).
[14] M. Mori, T. Ishimasa, and Y. Kashiwase, Philos. Mag. Lett. **64**, 49 (1991).
[15] M. J. Capitan, M. Bessière, S. Lefebvre, Y. Calvayrac, A. Quivy, and D. Gratias, in *Quasicrystals*, edited by C. Janot and R. Mosseri (World Scientific, Singapore, 1995), p. 173.
[16] R. Caudron, A. Finel, Y. Calvayrac, M. Fradkin, and R. Bellissent, in *Quasicrystals* (Ref. 15), p. 652.
[17] S. Lequien, L. Goirand, and F. Lesimple, Rev. Sci. Instrum. **66**, 1725 (1995).
[18] J. W. Cahn, D. Shechtman, and D. Gratias, J. Mater. Res. **1**, 13 (1986).
[19] The silicon sample was previously chemically polished to eliminate any residual surface stress. The silicon surface is perpendicular to the (1,1,0) direction and the presented map corresponds to a mesh scan of the Si(1,1,1) Bragg peak along the $[\bar{1}, 1, 0]$ zones axis. The configuration has been carefully chosen in order to have a resolution of the setup equivalent to the one used in the study of the quasicrystal samples.
[20] Several scans of Bragg peaks and diffuse intensity have been made for both samples in this setup in order to confirm that the differences in intensity are not due to the change in resolution. From these scans it is clear that the integrated Bragg peak intensities are preserved but that the diffuse scattering is different.
[21] E. E. Fullerton, I. K. Schuller, H. Vanderstraeten, and Y. Bruynseraede, Phys. Rev. B **45**, 9292 (1992).
[22] P. R. Bevington, *Data Reduction and Error Analysis for the Physical Sciences* (McGraw-Hill, New York, 1968), p. 105.
[23] The origin of the difference in the quality in the fit between the two samples can be related to the *q*-decay behavior of the diffuse intensity around the Bragg peaks: Sample 1 shows a much faster *q*-decay than sample 2. This could indicate that the approximation made in the expression of the hydrodynamical matrices of taking into account only the first term of a Taylor expansion is not well adapted in the case of samples with very low diffuse intensity.